



## OPEN ACCESS

## EDITED BY

Xiaohuan Zhao,  
Jinan University, China

## REVIEWED BY

Yinjie Ma,  
Hunan University, China  
Jiaqiang E,  
Hunan University, China

## \*CORRESPONDENCE

Weihuang Zhong,  
✉ 221076847@stdmail.gxust.edu.cn

RECEIVED 07 April 2023

ACCEPTED 08 May 2023

PUBLISHED 30 May 2023

## CITATION

Li J, Zhong W, Zhang J, Zhao Z and Hu J (2023), The combustion and emission improvements for diesel–biodiesel hybrid engines based on response surface methodology. *Front. Energy Res.* 11:1201815. doi: 10.3389/fenrg.2023.1201815

## COPYRIGHT

© 2023 Li, Zhong, Zhang, Zhao and Hu. This is an open-access article distributed under the terms of the [Creative Commons Attribution License \(CC BY\)](https://creativecommons.org/licenses/by/4.0/). The use, distribution or reproduction in other forums is permitted, provided the original author(s) and the copyright owner(s) are credited and that the original publication in this journal is cited, in accordance with accepted academic practice. No use, distribution or reproduction is permitted which does not comply with these terms.

# The combustion and emission improvements for diesel–biodiesel hybrid engines based on response surface methodology

Junming Li<sup>1</sup>, Weihuang Zhong<sup>2,3\*</sup>, Jian Zhang<sup>2</sup>, Ziheng Zhao<sup>3</sup> and Jingyi Hu<sup>2,3</sup>

<sup>1</sup>School of Electronic Engineering, Guangxi University of Science and Technology, Liuzhou, China, <sup>2</sup>Guangxi Earthmoving Machinery Collaborative Innovation Center, Guangxi University of Science and Technology, Liuzhou, China, <sup>3</sup>Guangxi Key Laboratory of Automobile Components and Vehicle Technology, Guangxi University of Science and Technology, Liuzhou, China

With the rapid technological progress of society and increasingly stringent environmental regulations, further reduction of emissions has become an important issue for environmental protection. This study developed a response surface model with the biodiesel blending ratio (BBR), load, and exhaust gas recirculation (EGR) as independent variables and brake thermal efficiency (BTE), brake specific fuel consumption (BSFC), and NO<sub>x</sub>, and CO emission rates as dependent variables. Simulations were performed and calculated. The results of the response surface approach with the objectives of maximizing the BTE of the engine and minimizing BSFC, NO<sub>x</sub> emissions, and CO emissions show that when the BBR is 20%, the EGR rate is 15%, and the engine load is 74.52%, pollutant emissions are significantly reduced while the engine power's performance is maximized.

## KEYWORDS

optimization, response surface methodology, engines, diesel–biodiesel, emissions

## 1 Introduction

The efficient use of energy and environmental sustainability has become the focus of attention in many countries (Alaswad et al., 2015; Yu et al., 2016). Biodiesel is not only a renewable energy source (Martos et al., 2016; Zhang et al., 2022d) but also can effectively improve the combustion of diesel engines (Khare et al., 2011; Foley et al., 2013) and increase the thermal efficiency and reduce the emission of pollutant gases from diesel engines (Cui et al., 2017; Zhang et al., 2022c). The most direct way of reducing emissions from diesel engines is through after-treatment, which can significantly reduce the emissions of exhaust gases. For example, Zhao investigated the optimum operating conditions of a diesel particulate filter (DPF) at different temperatures, oxygen concentrations (Zhao et al., 2023), and exhaust gas loads (Zhao et al., 2022), and compared the effects of different parameters on after-treatment. Nowadays, the research on the combustion characteristics (Zhang et al., 2023a) of biodiesel in diesel engines is increasing (E et al., 2017; Cai et al., 2023). In recent years, many studies on diesel combustion (Zhang et al., 2021a) and diesel combustion after-treatment (Zhao et al., 2021) have been conducted. However, few experiments analyze and optimize each input parameter of diesel engines because many

different results are usually produced, and the experiments need to be fully analyzed to produce the desired data. Different experimental analysis methods often result in different test protocols (Nuchitprasittichai and Cremaschi, 2011). Each method of experimental analysis in the engine field has distinct advantages and disadvantages (Zhang et al., 2022e; Tan et al., 2023b).

The orthogonal design of experiments method is a method that uses extreme difference analysis and analysis of variance, mainly through orthogonal tables, to arrange experiments characterized by simple operation and low workload (Shi et al., 2023). The orthogonal experimental method has a wide range of adaptability and is applied in various fields such as engineering, materials science, physics, and other multifaceted applications (Zhang et al., 2022a; Zhang et al., 2022b). Wang et al. (2022) studied the effect of combustion parameters on the combustion characteristics and NO emission characteristics of combustion in a combustion furnace by orthogonal experiments and concluded that the deflection angle of the blade end had a significant effect on the furnace temperature and NO emissions. The number of blades had no effect on the furnace temperature and NO emissions. Li et al. (2022) proposed a timing of the design energy consumption relationship of a typical rural house in a severely cold region. The optimization method is a multi-factor, multi-objective optimization using the orthogonal experiment method and the optimization method with entropy weights. A design scheme is proposed after comparing 18 optimization schemes that effectively improve the subjective design flaws of the constructors during building design and increase energy saving, cost-benefit ratio, and carbon emission reduction considerations. Hu et al. (2022b) proposed a method in response to the problems of increasing form factor and deterioration of key performance indexes by structural optimization methods used in the design process of magnetorheological (MR) valves. A geometric optimization design method is proposed for the optimal design of MR valve structures under specific volume constraints. In this work, a second-order response surface methodology (RSM) model is proposed to fit the radial flow path and spool region density of the radial MR valve using orthogonal experiments and response surface analysis, and the accuracy of the response surface function is also estimated for the entire design development. Finally, a geometric optimization problem was formulated for the constructed RSM using a genetic algorithm to find the global optimal geometric parameters of the radial MR valve, and the correctness of the algorithm and the effectiveness of the optimized design were effectively verified by experiments (Li et al., 2023b). Conducting experiments according to an orthogonal design method allows effective comparison of preselected parameters to determine their degree of influence on the experimental results. Sometimes, the actual determination of the specific optimization range requires the intervention of other optimization methods to complement the accuracy of the experimental results; ANOVA lacks the means to portray a nonlinear relationship between multiple factors.

The genetic algorithm (GA) is a method for solving optimization problems. The adaptation function is used to measure the overall situation to achieve the optimal solution, and the genetic algorithm has a stronger global search capability by randomly selecting individuals, which can avoid falling into the local optimal solution, and has higher solution accuracy. Teng and Qin (2019)

In order to study the relationship curves of torque with soot and  $\text{NO}_x$  under the premise of satisfying the torque output demand and soot emission demand, the relationship curves of torque with soot and  $\text{NO}_x$  are determined using the established genetic algorithm model penalty function, and the best combination of ECG parameters and fuel supply parameters is found by optimization. A genetic algorithm based on algebraic analysis is proposed to optimize the combustion phase change angle of a dual-fuel engine, and a double Wiebe function is proposed to fit the actual operating conditions in its work. Finally, by comparing the genetic algorithm with the Levenberg–Marquardt (LM) algorithm for iterative calculations, the genetic algorithm is examined for its practicality, and also, the accuracy of the genetic algorithm is demonstrated (Hu et al., 2022a). However, while improving its convergence, the genetic algorithm requires about 150 iterations, requiring much computational time. Li et al. (2023a) proposed a non-dominated ranking genetic algorithm (NSGA III) that has been recently investigated. This genetic algorithm differs from the traditional NSGA II in that NSGA III employs a diversity maintenance strategy that uses a set of uniformly distributed reference points to preserve the diversity of communities. This approach is better than NSGA II, which uses a crowded ranking of reference points and is more applicable to multidimensional problems. Moreover, the reference points in NSGA III results can directly identify similar individuals, and the optimal solution can be found in a shorter time during the enhanced training. Compared with previous genetic algorithms, the proposed algorithm greatly facilitates the processing of optimization results, increases accuracy, and limits the consumption of computational time. However, due to the varying degree of crowding of the initial data, some genetic algorithms may lead to data misuse; some local optimal solutions are ignored by mistake, thus losing the optimal solutions. Some additional processing is needed to improve or supplement the genetic algorithm (Hu et al., 2022a).

The RSM can be used to solve the interaction between random variables and system response variables through advanced experimental design methods (Solmaz et al., 2021; Liu et al., 2023). The main components of response surface experimental methods include experimental design and function fitting, and their accuracy is mainly determined by the design of the response surface function and the values of the coefficients in the function (Singh et al., 2021). RSM has been applied to develop models using design of experiments and multiple linear regression analysis techniques (Ozgur, 2021). The established second-order RSM model has been found to be the most appropriate in the current work. Currently, the RSM is widely used in engineering practice and has been studied by many experts worldwide in the field of internal combustion engine combustion. Kashyap et al. (2021) obtained the best performance of the dual fuel engine by replacing 20% of the hydrogen at higher loads by using RSM. The analysis of variance (ANOVA) of the experimental results at the 95% confidence level showed that the developed model was significant. Simsek and Uslu (2020) investigated the effect of biodiesel/2-ethylhexyl nitrate (EHN) fuel blends on diesel engine performance and emissions by RSM. In the RSM model created, three continuous factors were selected to create a Pareto chart supporting the analysis of variance and the validity of the selected input factors was determined. The final optimum values for the engine parameters were derived as

100% biodiesel percentage, 1.1% EHN percentage, and 1515 W load. The results show that the response surface experimental approach can effectively optimize compression ignition engine performance and exhaust emissions powered by a combination of biodiesel and EHN, thus saving time and reducing engineering effort. [Yilmaz et al. \(2022\)](#) studied diesel fuel blends and considered that the addition of 1-pentanol to biodiesel blends will increase the use of alternative fuels in diesel engines. The RSM was used to optimize the biodiesel blending ratio (BBR) and study the effect of these three component blends on emissions by considering the relationship between brake thermal efficiency (BTE), brake specific fuel consumption (BSFC), CO, HC, and NO<sub>x</sub> in relation to the three additive ratios to find the optimal blending ratio of 79.9% diesel, 8.33% waste oil biodiesel (WOB), and 12.58% 1-pentanol to achieve the best emission economy. The results of these studies help understand the combustion reaction process of diesel–biodiesel dual-fuel engines and have some engineering guidance for energy saving and emission reduction of dual-fuel diesel engines.

Biodiesel is a popular alternative fuel with the advantages of lean combustion, high octane number, and latent heat of vaporization, which can improve the combustion and emission characteristics of engines without changing the engine structure. It is essential to find the right combination of the advantages of the engine's exhaust gas recirculation (EGR) and biodiesel fuel that will meet the emissions and engine performance targets. At present, researchers mostly use single factors for combustion and emission characteristics analysis of biodiesel, but parameters usually interact with each other, so it is necessary to use multi-objective optimization methods. RSM is an optimization method that can be used to reduce the number of experiments and to accurately predict the optimal operating parameters of the engine. Therefore, this paper uses the RSM with the objectives of maximizing BTE and minimizing BSFC, NO<sub>x</sub>, and CO to derive the optimal biodiesel blending ratio, the optimal workload, and the optimal EGR.

## 2 Materials and method

### 2.1 Preparation and characterization of test fuels

Biodiesel can achieve good combustion conditions in engines due to its high octane number and high latent heat of vaporization. Experiments were conducted using different proportions of biodiesel to investigate the blending ratio. The specific experiments are described as follows.

#### 2.1.1 Main parameters and boundary conditions of the model

The temperature boundary conditions are given empirically and are set as follows: piston temperature is 553 K, cylinder head temperature is 523 K, cylinder wall temperature is 373 K, and injection nozzle temperature is 550 K. Velocity boundary conditions: piston movement speed is the actual piston movement speed at the calculated speed, and the remaining components are stationary. The turbulent kinetic energy (TKE) and turbulence length scale (TLS) in the initial combustion

TABLE 1 Relevant parameters of the model.

Parameter	Value
Bore × stroke (mm)	190 × 210
Connecting rod (mm)	410
Engine speed (r/min)	1,000
Number of fuel injection holes	8
Nozzle radius (mm)	0.28
Initial cylinder turbulence energy (m <sup>2</sup> /s <sup>2</sup> )	18.375
Compression ratio	14
Inlet initial pressure (MPa)	0.193
Effective power (kW)	220
Spray angle (°)	150

chamber are calculated from the following equations ([Zhang et al., 2021b](#)):

$$TKE = \frac{3}{2} \times u, \quad (1)$$

$$u = 0.7 \times 2 \times h \times \frac{n}{60}, \quad (2)$$

$$TLS = \frac{h_v}{2}, \quad (3)$$

where  $u$  indicates turbulent pulsation velocity, mm/s;  $h$  is the diesel engine stroke, mm;  $n$  is the diesel engine speed, rpm;  $h_v$  is the maximum valve lift, mm.

The main parameters of the diesel engine are shown in [Table 1](#).

#### 2.1.2 Fuel properties

The study examined diesel/biodiesel blends with different biodiesel blending ratios, namely, D95B5, D90B10, D85B15, and D80B20, respectively. D95B5 represents 95% diesel +5% biodiesel, D90B10 represents 90% diesel +10% biodiesel, D85B15 represents 85% diesel +15% biodiesel, and D80B20 represents 80% diesel +20% biodiesel. The input physical properties of the model are treated as constant values, and the physicochemical properties of diesel and biodiesel are shown in [Table 2](#) ([Chen et al., 2012](#); [Tan et al., 2023a](#)).

#### 2.1.3 Experimental setup

The experimental arrangement is shown in [Figure 1](#): the fuel is controlled by an oil pressure sensor (accuracy ±1% MPa) at the outlet, and at the end of the test setup, the emission levels of NO<sub>x</sub> and CO in the exhaust gas are measured with an exhaust gas analyzer with an accuracy of ±5 ppm. The models measured by the sensor during the experiment are passed through the computer to the electronic control unit and finally to the computer for analysis.

#### 2.1.4 Verification of grid independence

Before the model can be simulated, the accuracy of the simulation was verified using a suitable mesh density. [Figure 2](#) shows the cylinder pressure curve with different grid sizes that can ensure accuracy and reduce the calculation time. A grid size of 2 mm was chosen for the experimental study.

TABLE 2 Physiochemical properties of diesel and biodiesel.

Fuel	Diesel	Biodiesel (RME)	D95B5	D90B10	D85B15	D80B20
Flash point temperature (°C)	67	168	72.05	77.1	82.15	87.2
Oxygen volume fraction (%)	0.0	10.7	0.535	1.07	1.605	2.14
Density (g/m <sup>3</sup> , at 20°C)	0.82–0.86	0.882	0.8231–0.8611	0.8262–0.8622	0.8293–0.8633	0.8324–0.8644
Latent heat of vaporization (kJ·kg <sup>-1</sup> )	253.31	273.36	254.31	255.315	256.32	257.32
Viscosity (MPa·s, at 20°C)	3.0–8.0	4.556	3.08	3.16	3.23	3.31
Cetane number (CN)	45–66	53.88	45.444	45.888	46.332	46.776
Low heating value (MJ·kg <sup>-1</sup> )	42.5	39.53	42.3515	42.203	42.0545	41.906

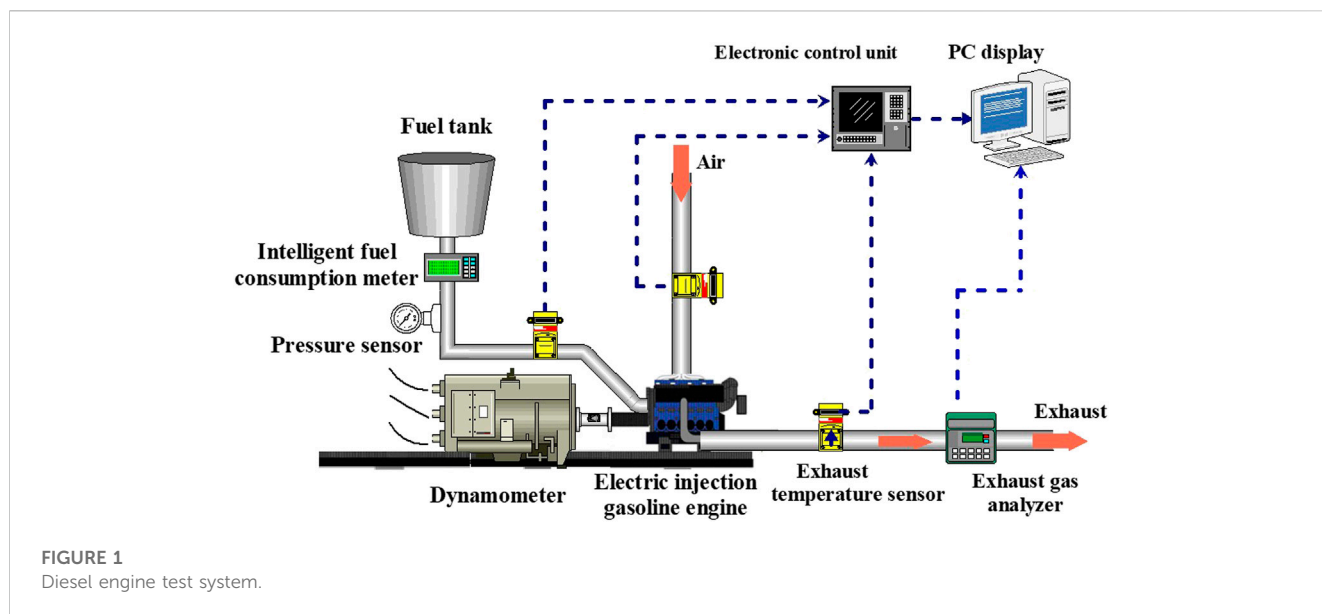


FIGURE 1 Diesel engine test system.

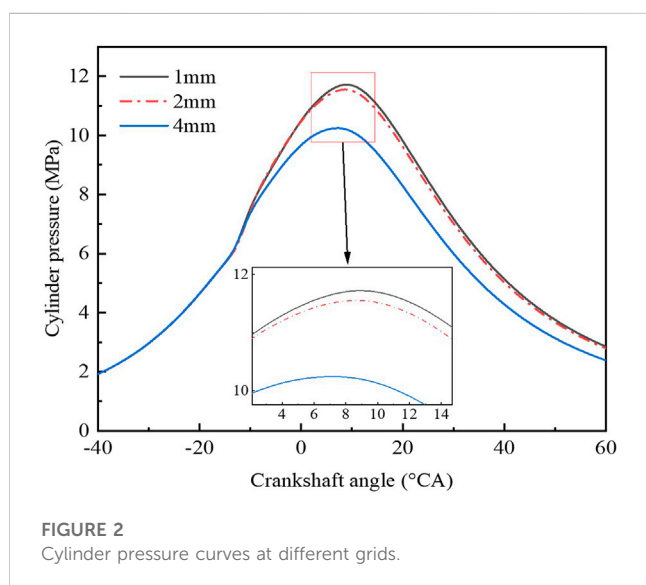


FIGURE 2 Cylinder pressure curves at different grids.

### 2.1.5 Experimental verification

The experimental and simulation results were compared for cylinder pressure, heat release rate (HRR), and trends on NO<sub>x</sub> emissions at 100% and 50% load. As shown in Figure 3, both the experimental and prediction errors were within 5%, and the accuracy of the model was verified by the experiment. It was concluded that the model was accurate.

### 2.2 Response surface optimization method calculation formula

The research route of the RSM is to set up a finite number of representative experiments by experimental design and use the least squares method to derive polynomials to express the state function of the implicit limit based on the experimental output. Overall, the RSM is a practical statistical method to determine the final best response value between different inputs (Yusup et al., 2014; Sun et al., 2017).

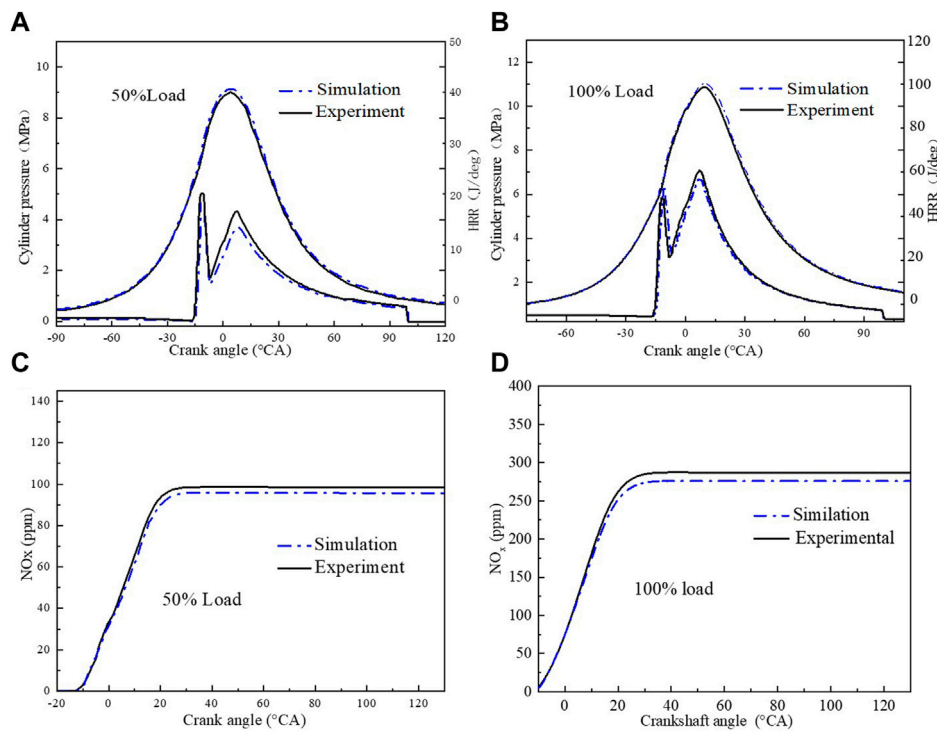


**FIGURE 3** Comparison of experimental and simulated data at 100% and 50% load conditions: (A) indicates cylinder pressure at 50% load, (B) indicates cylinder pressure at 100% load, (C) NO<sub>x</sub> concentration at 50% load, and (D) NO<sub>x</sub> concentration at 100% load.

In order to derive quantitative relationships between the three structural parameters of BBR, load, and EGR and the economic performance indicators (BTE and BSFC) and emission indicators (NO<sub>x</sub> and CO), a response surface function was constructed based on the RSM with the objectives of maximizing BTE and minimizing BSFC, NO<sub>x</sub> emissions, and CO emissions. The basic equations are as follows:

$$y = \alpha_0 + \sum_{a=1}^n \alpha_a x_a + \sum \sum_{a < b} \alpha_{ab} x_a x_b + \sum_{a=1}^n \alpha_{aa} x_a^2 + \epsilon, \quad (4)$$

where  $y$  denotes the response value;  $\alpha_0$ ,  $\alpha_a$ ,  $\alpha_{aa}$ , and  $\alpha_{ab}$  denote the regression coefficients of different factors;  $x_a$  denotes the values of different factors;  $\epsilon$  denotes the random error.

Among them, the relationship between the number of basic functions  $Y$  and the number of design parameters  $\mu$  is divided into linear, quadratic polynomial, and cubic polynomial relationships.

$$Y = \mu + 1, \quad (5)$$

$$Y = \frac{(\mu + 1) \times (\mu + 2)}{1 \times 2}, \quad (6)$$

$$Y = \frac{(\mu + 1) \times (\mu + 2) \times (\mu + 3)}{1 \times 2 \times 3}. \quad (7)$$

### 2.3 Significance test model

The adaptability and accuracy of the model must be quantified to assess the predictive power of the model and perform significance

tests on the established response surface models. Many factors determine the accuracy of the response surface model: the number of data groups collected, the smoothness of the actual function, and the choice of the response surface equation. In this paper, error analysis is performed statistically. The sum of squares of multiple error fluctuations and the value of degrees of freedom are used in statistics to test the response surface model (Jamaluddin et al., 2013). The specific equations are as follows:

$$M_i = \sum_{a=1}^N (y_a - \bar{y})^2 \quad G_i = N - 1, \quad (8)$$

$$M_j = \sum_{a=1}^N (y_a - \bar{y})^2 \quad G_j = N - n, \quad (9)$$

$$M_k = \sum_{a=1}^N (y_a - \bar{y})^2 \quad G_k = n - 1, \quad (10)$$

$$\bar{y} = \frac{1}{N} \sum_{a=1}^N y_a, \quad (11)$$

where  $y_a$  and  $\bar{y}$  are the true and approximate function values of the sample  $G$ , respectively;  $N$  is the number of design parameters;  $n$  is the number of functions;  $M_i$  and  $G_i$  are the total sum of squares and degrees of freedom of error fluctuations;  $M_j$  and  $G_j$  are the degrees of freedom and sum of squares of residual fluctuations, respectively;  $M_k$  and  $G_k$  are the sum of squares and degrees of freedom of fitted error fluctuations, respectively. Thus, the F-value used to test the accuracy of the response surface model can be obtained based on the probability statistical theory.

TABLE 3 Response surface design simulation data.

BBR (%)	EGR (%)	Load (%)	BSFC (g/(kW·h))	BTE (%)	NO <sub>x</sub> (ppm)	CO (ppm)
5	0	100	405.97	35.33	272	79.23
5	0	50	333.63	28.62	96.035	14.53
5	10	50	306.25	27.23	65.32	34.36
5	0	75	274.07	32.86	189.947	45.36
5	10	75	283.76	31.56	125.23	65.23
5	10	75	283.76	31.56	125.23	65.23
5	15	100	439.23	34.92	110.23	112.36
10	15	50	272.36	30	38.56	32
10	5	100	436.23	34.68	198.32	80.12
15	0	50	326.30	28.88	97.641	26.56
15	0	75	269.77	33.32	190.70	46.53
15	10	50	302.35	28.06	43.04	23.56
15	0	75	269.77	33.12	190.70	46.53
15	10	100	446.23	35.32	125.36	58.65
15	10	100	446.23	36.32	125.36	58.65
15	0	75	269.77	32.5	190.70	46.53
20	5	50	308.02	30.76	50.23	23.86
20	15	75	275.62	33.12	24.6	17.02
20	15	75	275.62	33.12	24.6	17.02
20	0	100	401.11	36.7675	263.25	60.78

$$F(G_k, G_j) = \frac{G_c \times M_k}{G_k \times M_j}, \quad (12)$$

$$F(G_k, G_j) > F_a(G_k, G_j), \quad (13)$$

where  $R^2$  is used as a complex correlation coefficient to test the accuracy criteria of the model. Its calculation equation is as follows:

$$R^2 = \frac{G_k}{G_i}. \quad (14)$$

$R^2$  can measure the fit of the established response surface model, and in general, the closer  $R^2$  to 1, the higher the accuracy of the model fit (Cui et al., 2022). However, when the number of design variables and basis functions in the response surface model gradually increases, it will appear that  $R^2$  will be close to 1, which cannot be used to evaluate the fitting accuracy, so  $R^2_{Adj}$  (adjustment factor) is proposed as follows:

$$R^2_{Adj} = 1 - \frac{M_j \times G_i}{M_i \times G_k}. \quad (15)$$

## 2.4 Response surface model construction

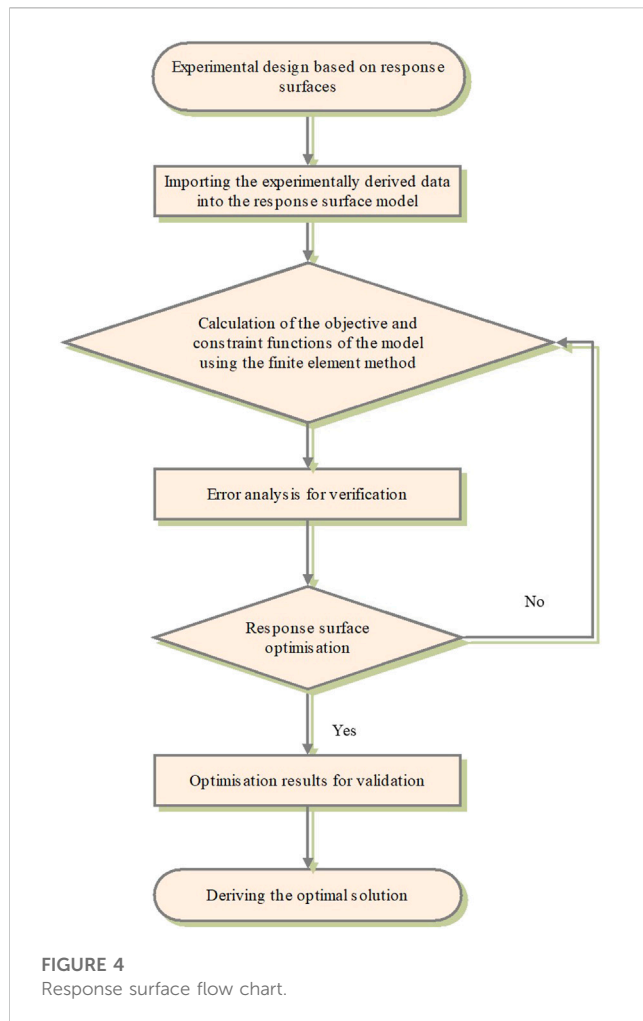
In this paper, a response surface model is established based on the diesel engine operating parameters. On the premise of ensuring

high model accuracy, the response surface optimization is carried out, and the optimal operating parameters of the diesel engine are derived. The specific process is shown in Figure 4.

The Design-Expert software was used to create the response surface experimental design, and 20 sets of experimental data were derived. A response surface model was developed with BBR, load, and EGR as independent variables and BTE, BSFC, NO<sub>x</sub> emissions, and CO emission as dependent variables, and simulations were performed to calculate the results shown in Table 3.

The core of the response surface optimization analysis method is to design the appropriate parameter variables in the space with a suitable experimental design method (Shahbaz et al., 2016). The input parameters are substituted into the response surface model, and the multiple quadratic regression equation is used to fit the direct mathematical function relationship between the influencing factors and the response results according to the input and output parameters, and then, the measured response value is used as the target value to obtain the ideal value with the response surface model.

In this article, a quadratic regression model of the engine system is represented to analyze the biodiesel blending ratio, the workload, and the effect of EGR on engine combustion and emissions. The difference between the predicted and target values is called the residual. Figure 5 shows the predicted BSFC, BTE, and NO<sub>x</sub> emissions against the expected values. Figure 5 shows that the residuals of the model are very small, indicating that the fit and model are ideal.



### 3 Response surface parameter evaluation

#### 3.1 Brake-specific fuel consumption evaluation index

The fuel consumption model based on RSM is as follows (Elsayed and Lacor, 2011):

$$BSFC = 286.07 - 1.22A - B + 63.82C + 5.43AB + 4.06AC + 23.96BC - 1.56A^2 - 13.93B^2 + 91.34C^2. \quad (16)$$

The difference between the predicted value of fuel consumption calculated according to this formula and the simulated value is very small. *BSFC* is the brake-specific fuel consumption, g/(kWh); *A* is the BBR, %; *B* is the EGR rate, %; *C* is the engine load, %.

The variance analysis of fuel consumption is shown in Table 4. The biodiesel blending ratio, EGR, and biodiesel load have very significant effects on the model of fuel consumption ( $p$ -value of model < 0.0001). The response values of  $R^2$ ,  $R^2_{Adj}$ , and  $R^2_{Pre}$  (prediction factor) to the model are 0.9987, 0.9975, and 0.9912, respectively, which indicates that all squared terms are also significant for the model and can be used for the experimental prediction (Han et al., 2021).

Figure 6 shows the graphs of the biodiesel blending ratio, EGR, and load on fuel consumption individually for biodiesel. In Figure 6A, the biodiesel blending ratio has little effect on fuel consumption. The EGR curve in Figure 6B shows a smaller slope than the load. The graph of fuel consumption versus load shows that the effect of load is the main effect, and fuel consumption decreases then increases rapidly with increasing load, as depicted by a curve with a steep slope, as shown in Figure 6C.

Three-dimensional surface plots specifically depict the interaction between variables and responses. Figure 7 shows surface plots of the relationship between the biodiesel blending ratio and load about BSFC. The results show that engine load has a greater effect on power than blended fuel. The surface plot shows a drastic change when the load slightly changes from low to high. This higher load does more work leading to consuming more fuel. In addition, the image shows that the biodiesel percentage has a negligible effect on fuel consumption.

#### 3.2 Brake thermal efficiency evaluation index

The brake thermal efficiency model based on the RSM is as follows:

$$BTE = 31.88 + 0.56A - 0.15B + 3.45C + 0.02AB + 0.11AC - 0.09BC + 0.14A^2 + 0.76B^2 - 0.35C^2. \quad (17)$$

The error between the predicted and simulated values of brake thermal efficiency calculated by this formula is almost negligible. In the equation, *BTE* represents the BTE of the engine, %; *A* is the BBR, %; *B* is the EGR rate, %; *C* is the engine load, %.

The variance analysis of thermal efficiency is shown in Table 4. It can be seen from the table that the  $p$ -values of the biodiesel blending ratio, EGR, and load-to-fuel consumption of biodiesel are < 0.0001, 0.0865, and < 0.0001, respectively. Among them, the response values of  $R^2$ ,  $R^2_{Adj}$ , and  $R^2_{Pre}$  to the model are 0.9954, 0.9913, and 0.9761, respectively, which are all within the allowed error range. The predicted values of the model fit well in the experiment, which indicates that the model is correct and accurate. The model has a reference value for the prediction of thermal efficiency (Wang and Li, 2022).

Figure 8 shows the separate effects of biodiesel blending ratio, EGR, and load of BTE. In Figure 8, the biodiesel blending ratio has a positive correlation with the thermal efficiency in Figure 8A. The EGR has less effect on the BTE and remains around 32%, as shown by the curve in Figure 8B. As shown in Figure 8C, load is the main effect on the diesel engine, BTE increases rapidly with the increase of load, forming a curve with a steeper slope, and its effect on BTE is much greater than the biodiesel blending ratio and EGR. This indicates that as the load increases, diesel engine combustion in the cylinder becomes more and more adequate.

A 3D surface plot was created to further understand the interaction between the variables and the response. Figure 9 shows a surface plot of the relationship between the biodiesel blending ratio and load about BTE. The results show that the diesel load has a greater effect on BTE than the biodiesel blending ratio. A significant change can be seen on the surface plot when the load is changed slightly from low to high.

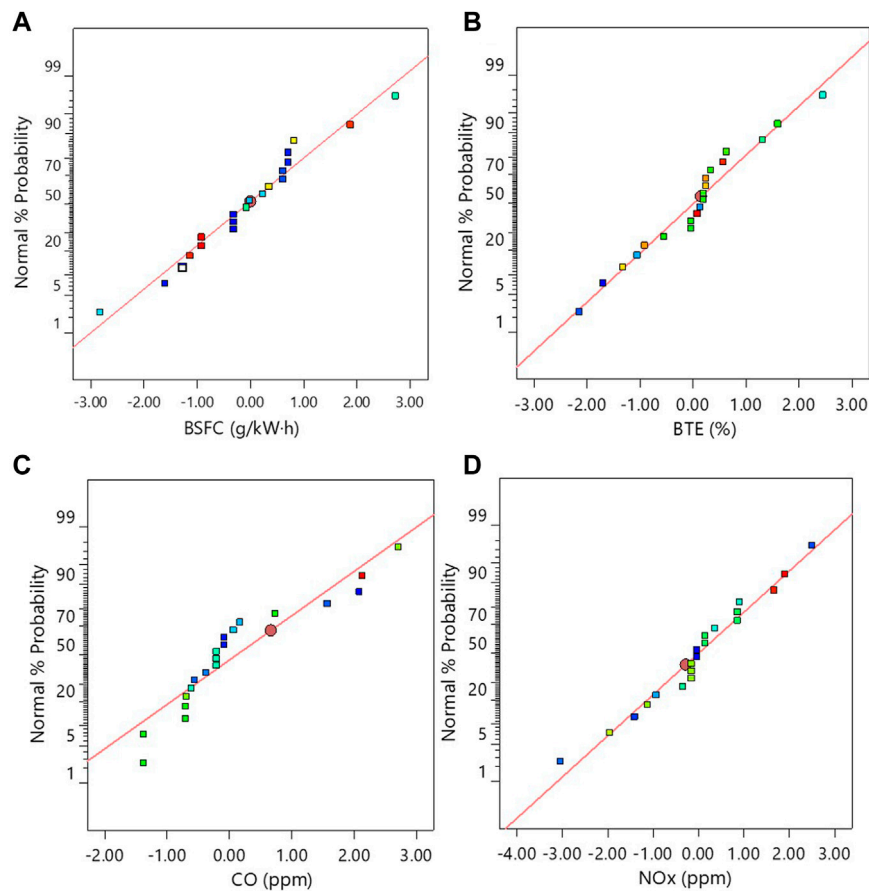


**FIGURE 5** BSFC, BTE, CO, and NO<sub>x</sub> forecast compared to the expected value: (A) BSFC, (B) BTE, (C) CO, and (D) NO<sub>x</sub>.

**TABLE 4** BSFC and BTE Miller’s cyclic ANOVA table.

	BSFC		BTE	
	F-value	p-value	F-value	p-value
Model	849.05	<0.0001	241.12	<0.0001
A	1.31	0.2791	47.51	<0.0001
B	0.9122	0.3620	3.61	0.0865
C	3,915.65	<0.0001	1937.09	<0.0001
AB	18.19	0.0016	0.0341	0.8572
AC	8.84	0.0140	1.17	0.3057
BC	307.93	<0.0001	0.7330	0.4119
A <sup>2</sup>	0.6656	0.4336	0.8859	0.3688
B <sup>2</sup>	50.28	<0.0001	25.28	0.0005
C <sup>2</sup>	3,065.10	<0.0001	7.94	0.0182
R <sup>2</sup>	0.9987		0.9954	
R <sup>2</sup> <sub>Adj</sub>	0.9975		0.9913	
R <sup>2</sup> <sub>Pre</sub>	0.9912		0.9761	

### 3.3 NO<sub>x</sub> evaluation index

The NO<sub>x</sub> model based on the RSM is as follows:

$$NO_x = 121.19 - 19.27A - 64.76B + 54.40C - 16.67AB - 1.28AC - 31.34BC - 2.09A^2 + 6.3B^2 - 10.32C^2. \tag{18}$$

The NO<sub>x</sub> of the diesel engine calculated according to this equation was obtained, and the error between the predicted and values simulated through calculation was almost negligible. Therefore, it can be considered that NO<sub>x</sub> obtained through the formula can represent the NO<sub>x</sub> emissions of the engine, ppm; A is the BBR, %; B is the EGR rate, %; C is the engine load, %.

The variance analysis of NO<sub>x</sub> is shown in Table 5. It can be seen that the model is significant and can express the state of the diesel engine and the corresponding effects in each case with basic accuracy. The p-values of BBR, EGR, and load on NO<sub>x</sub> are <0.0001. In addition, the response values of R<sup>2</sup>, R<sup>2</sup><sub>Adj</sub>, and R<sup>2</sup><sub>Pre</sub> to the model are 0.9991, 0.9983, and 0.9923, respectively. The high R-squared correlation coefficient ensures a satisfactory agreement between the calculated and observed data (Guo et al., 2012).



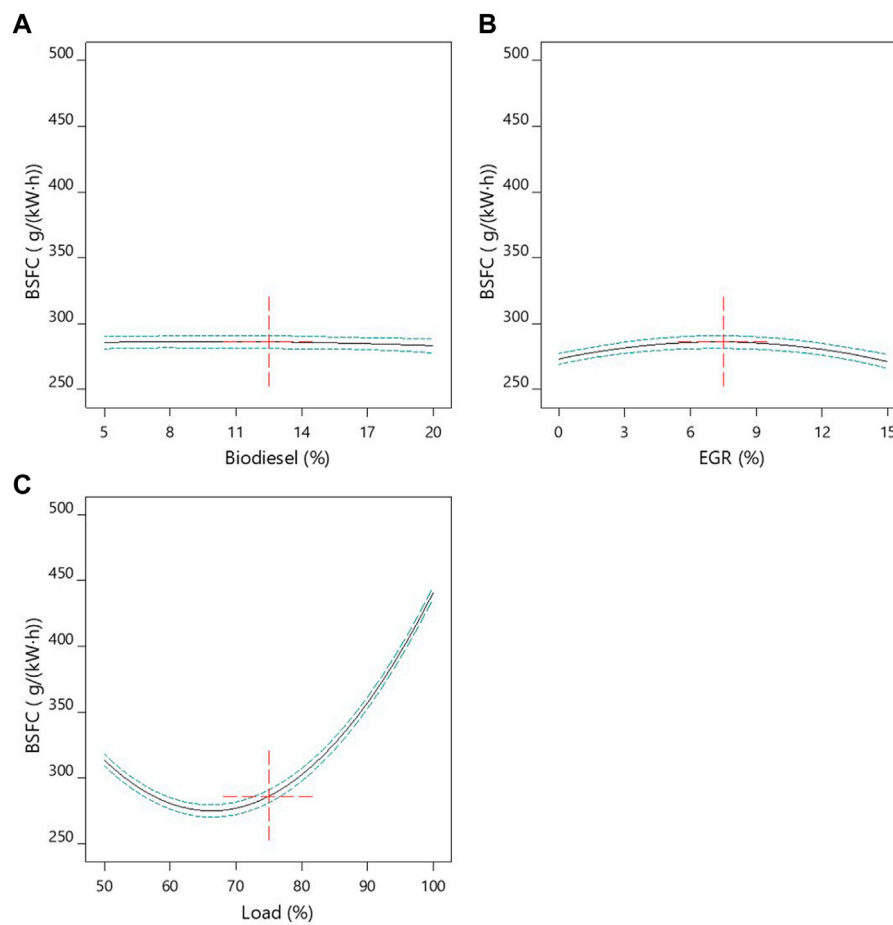


**FIGURE 6** Graph of the separate effects of the BBR, EGR, and load on fuel consumption: (A) biodiesel (%), (B) EGR (%), and (C) load (%).

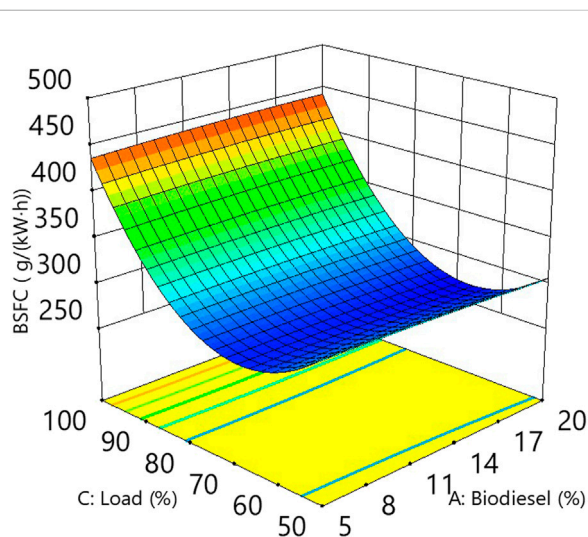
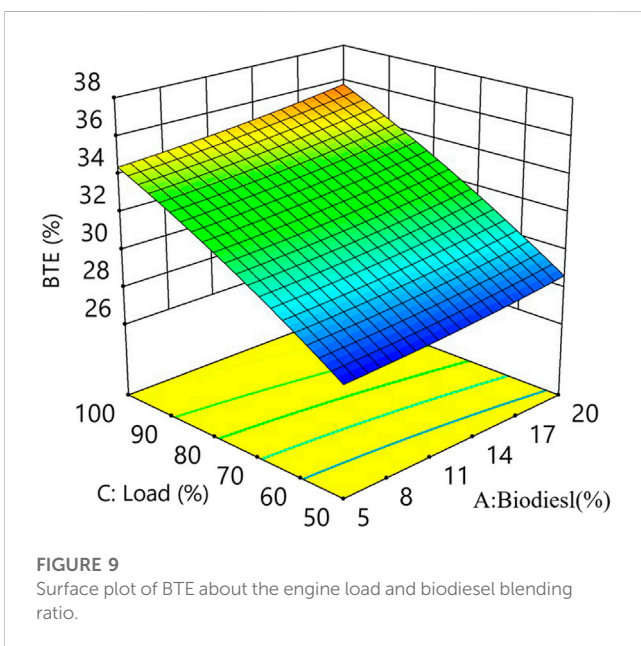
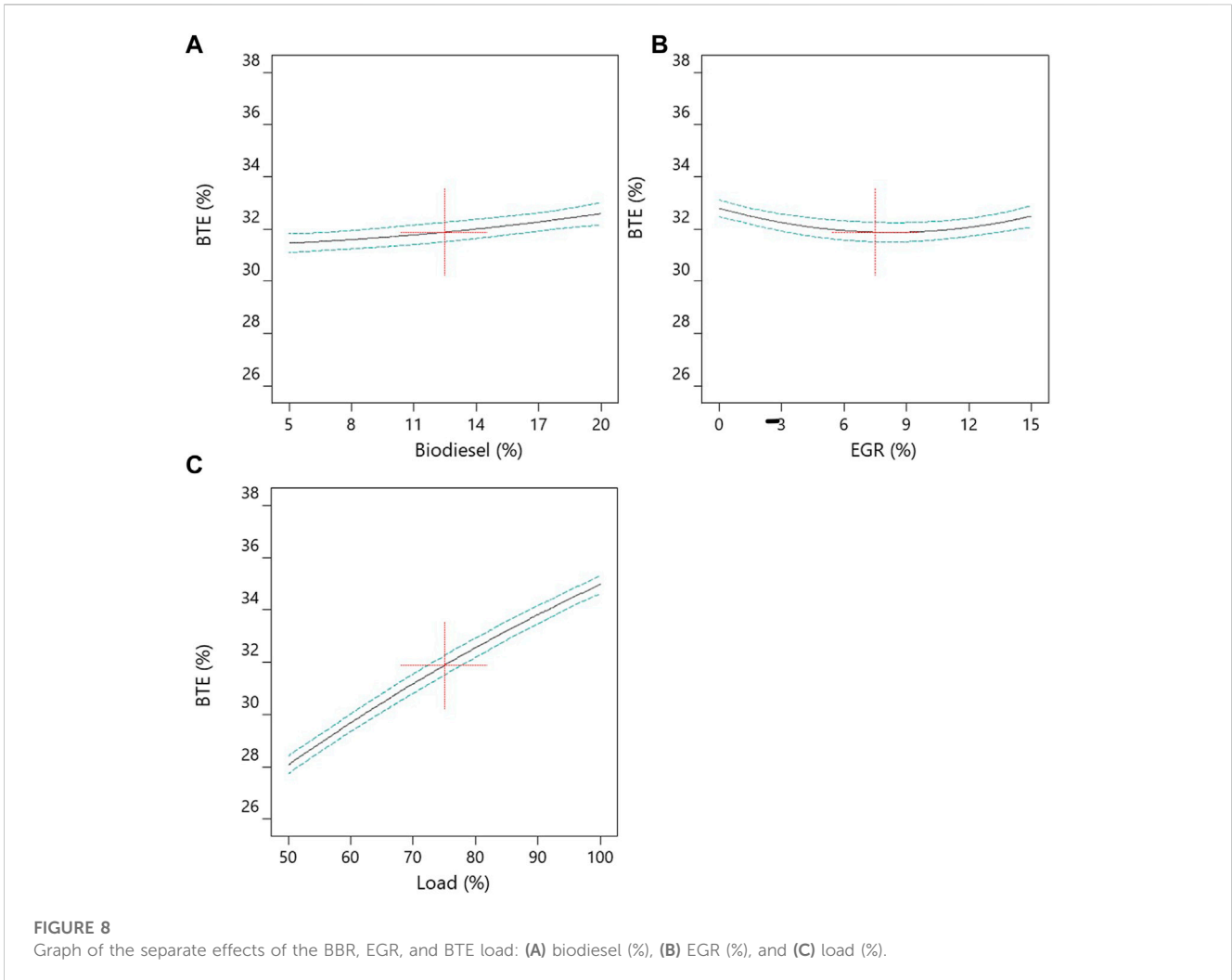


**FIGURE 7** 3D surface plot of BSFC about the engine load and biodiesel blending ratio.

The individual effects of the biodiesel blending ratio, EGR, and load on the  $\text{NO}_x$  emissions of a diesel engine are shown in Figure 10. The results show that the magnitudes of the effects on  $\text{NO}_x$  emissions are as follows: the EGR is the largest, followed by the biodiesel blending ratio, and the load has the least effect. As shown in Figure 10A, increases in the biodiesel blending ratio cause a moderate increase in  $\text{NO}_x$  emissions. This is because the high oxygen content of biodiesel leads to higher  $\text{NO}_x$ . As shown in Figure 10B, EGR is the most influential on  $\text{NO}_x$  emissions, and as EGR increases,  $\text{NO}_x$  decreases significantly. In addition, in Figure 10C, there is a negative correlation with the increasing load curve, and  $\text{NO}_x$  increases significantly with a large slope of the curve.

A 3D surface plot was created to further understand the interaction between the variables and the response. Figure 11 shows a surface plot of the relationship between EGR and load about thermal efficiency. The results show that  $\text{NO}_x$  emissions from the diesel engine decrease significantly as EGR increases, while  $\text{NO}_x$  emissions increase as the load and biodiesel blending ratio increase. The in-cylinder temperature increases significantly when the load changes from low to high, and the high temperature can lead to a large amount of  $\text{NO}_x$  formation.



### 3.4 CO evaluation index

The CO model based on the RSM is as follows:

$$CO = 46.08 - 15.09A + 0.45B + 22.81C - 15.10AB - 10.38AC - 0.45BC - 0.45A^2 + 0.81B^2 + 1.36C^2, \tag{19}$$

where  $CO$  represents the CO emissions of the diesel engine, ppm;  $A$  is the BBR, %;  $B$  is the EGR rate, %; and  $C$  is the engine load, %. The predicted values of CO for diesel engines can be calculated by this equation, and the obtained results have very little error with the simulated values, so the emission values of CO are calculated by this equation.

The analysis of variance for CO is shown in Table 5. In this case, the factors that affect the model are biodiesel blending ratio, EGR, and load. The F-value of the model was 505.73 with a  $p$ -value <0.0001, which is less than 0.05; thus, the model is significant. In addition,  $R^2$ ,  $R^2_{Adj}$ , and  $R^2_{Pre}$  were 0.9978, 0.9958, and 0.9755, respectively. The difference between the three was less than 0.2, implying that the model was appropriate (Zhang et al., 2023c).

TABLE 5 BSFC and BTE Miller's cyclic ANOVA table.

Gas	NO <sub>x</sub>		CO	
	F-value	p-value	F-value	p-value
Model	1,211.94	<0.0001	505.73	<0.0001
A	389.28	<0.0001	882.23	<0.0001
B	4,550.05	<0.0001	0.8137	0.3882
C	3,382.58	<0.0001	2,198.06	<0.0001
AB	203.97	<0.0001	618.56	<0.0001
AC	1.04	0.3313	253.97	<0.0001
BC	626.38	<0.0001	0.4896	0.5000
A2	1.42	0.2614	0.2442	0.6318
B2	12.24	0.0057	0.7637	0.4027
C2	46.61	<0.0001	2.98	0.1148
R <sup>2</sup>	0.9991		0.9978	
R <sup>2</sup> <sub>Adj</sub>	0.9983		0.9958	
R <sup>2</sup> <sub>Pre</sub>	0.9923		0.9755	

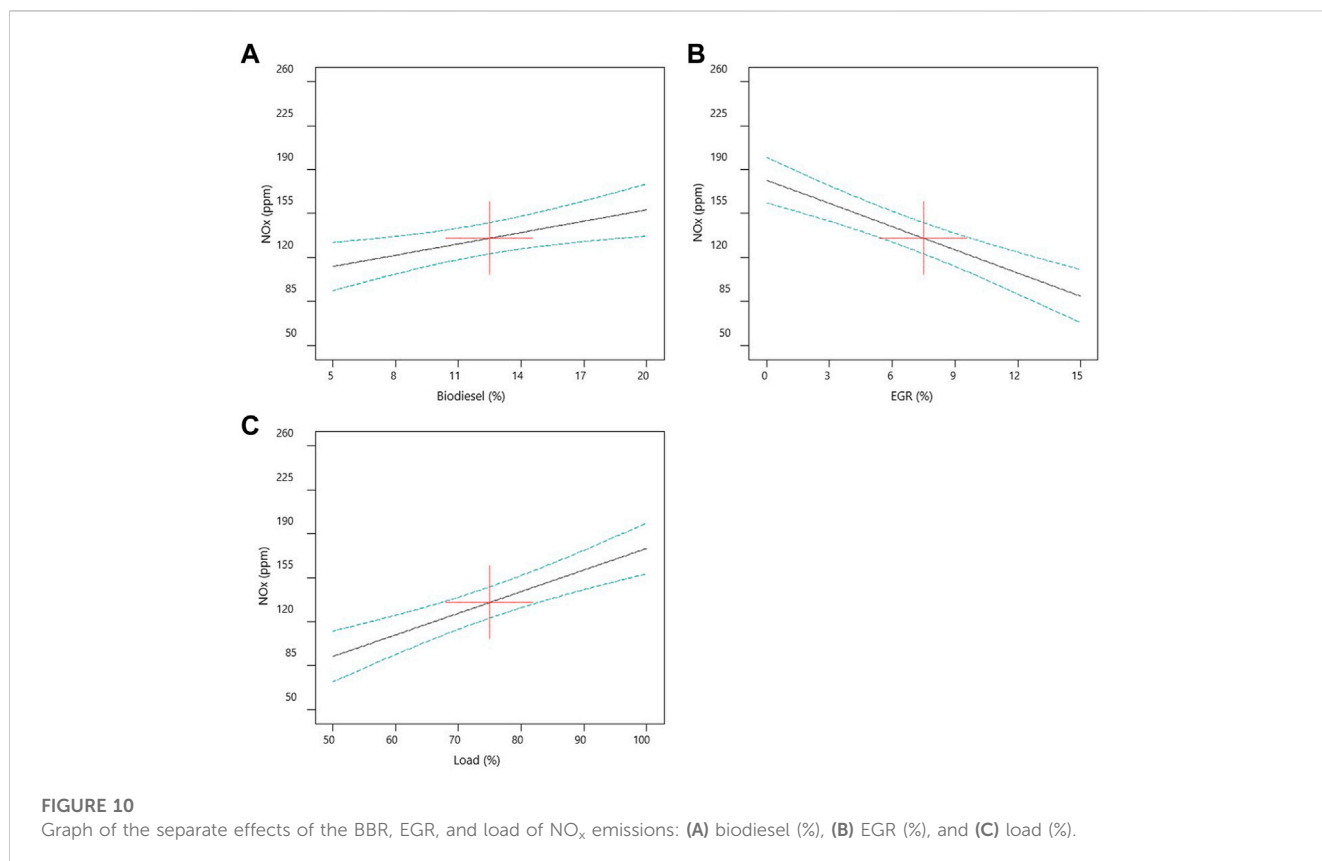
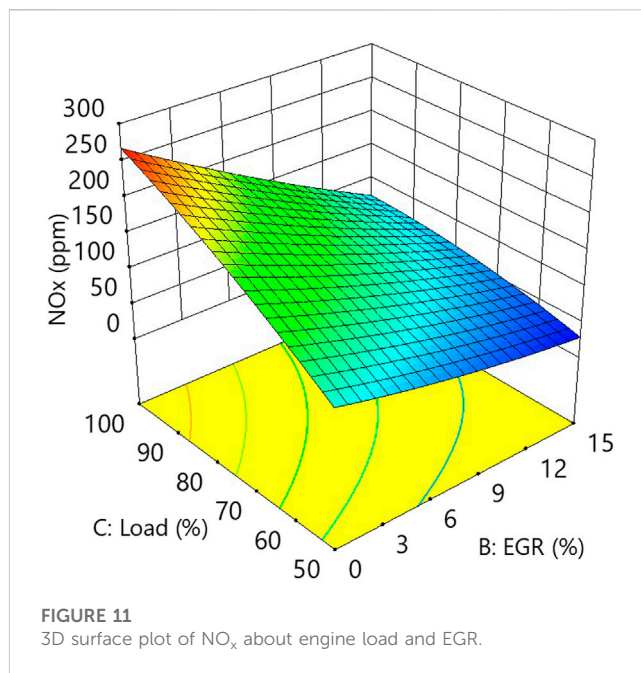
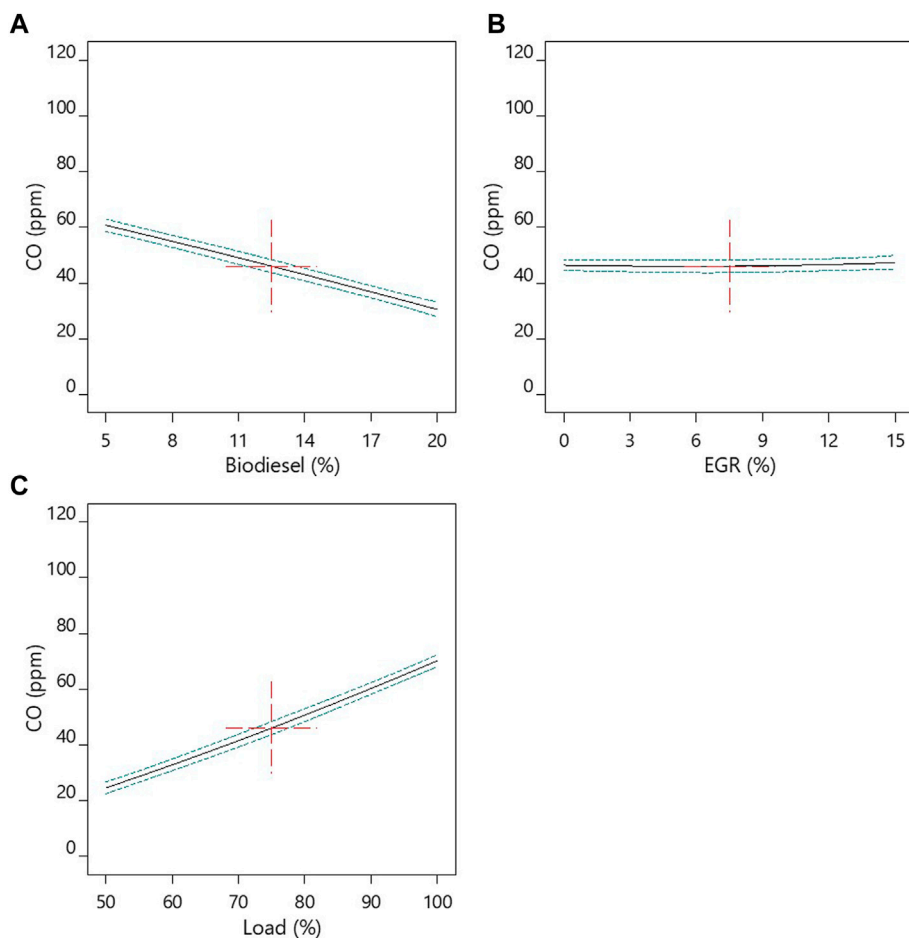


Figure 12 shows the individual effects of the parameters (Hu et al., 2023) on CO emissions. The increase in the oxygen content of biodiesel significantly increases the conversion of CO to CO<sub>2</sub>. As shown in Figure 12A, an increase in the biodiesel blending ratio

leads to a decrease in CO emissions, and its effect is prominent. EGR has little effect on CO emissions, as shown in Figure 12B. However, in Figure 12C, the load is an important factor affecting CO, and the increase of CO emissions as the diesel engine load increases may be



**FIGURE 12** Graph of the separate effects of the BBR, EGR, and load of CO emissions: (A) biodiesel (%), (B) EGR (%), and (C) load (%).

due to the increase of oxygen content, which leads to the increase in CO conversion to CO<sub>2</sub>.

A three-dimensional surface plot was created by analytical calculations. Figure 13 shows the surface plot of the relationship between the biodiesel blending ratio and load about BTE. Figure 13 shows that both the biodiesel blending ratio and load have a large effect on CO emissions. With the increased biodiesel blending ratio, the CO emissions of diesel engines decrease significantly, while with the increase of load, CO emissions also increase.

### 4 Multi-objective optimization

In this paper, BBR, load, and EGR are used as independent variables and BTE, BSFC, NO<sub>x</sub> emissions, and CO emissions are used as dependent variables to obtain the optimal parameters for multiple responses and to achieve the objectives of maximizing BTE and minimizing BSFC, NO<sub>x</sub> emissions, and CO emissions (Luo et al., 2022; Ye et al., 2023).

The best solution derived from the response surface multi-objective optimization was to use 20% canola oil with diesel fuel

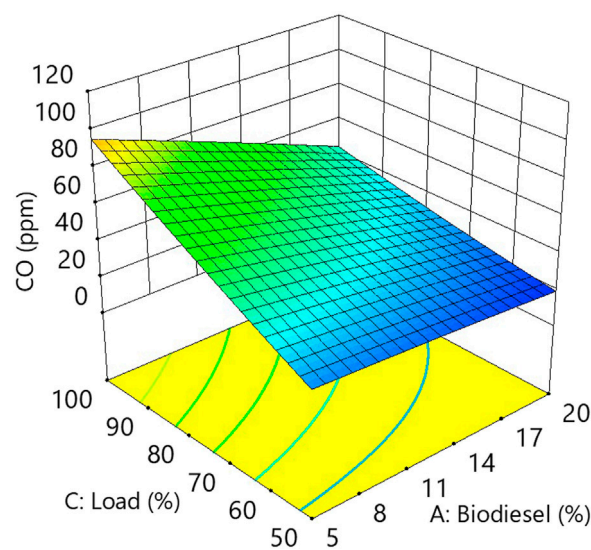


**FIGURE 13** 3D surface plot of CO about the engine load and biodiesel blending ratio.

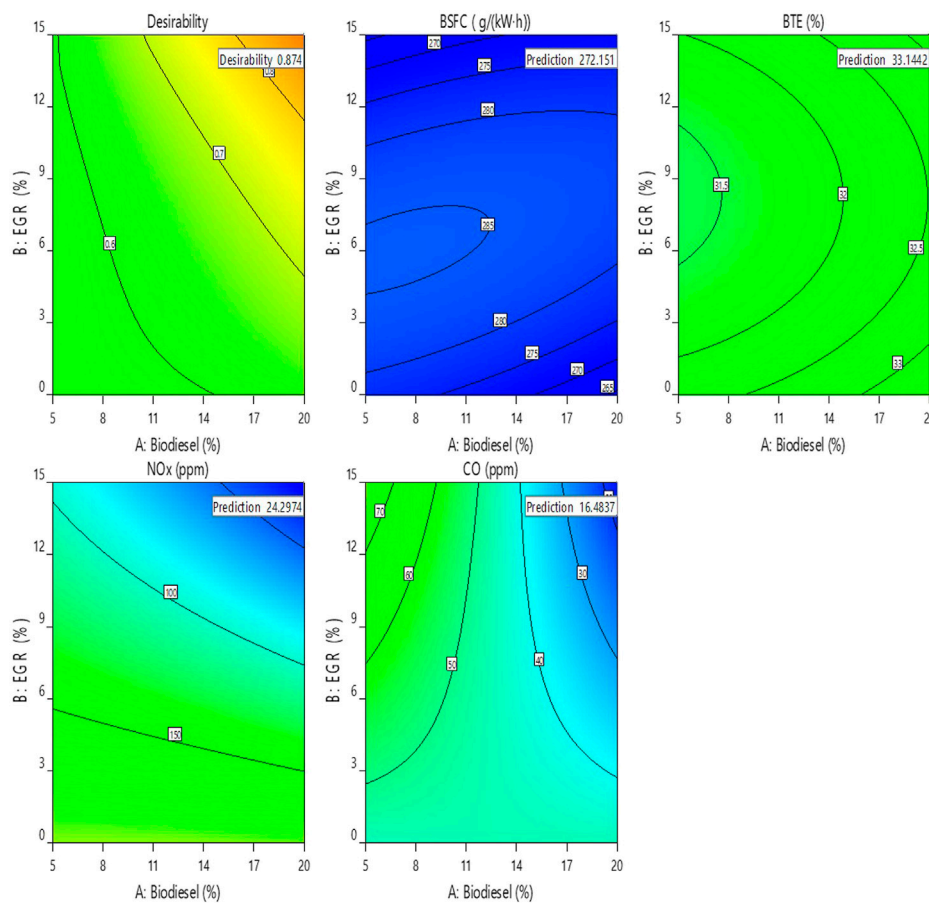


**FIGURE 14**  
Predicted value of the best engine operating conditions.

**TABLE 6 Validation of optimization results.**

BBR (%)	EGR (%)	Load (%)		Fuel consumption (g/(kW-h))	BTE (%)	NO <sub>x</sub> (ppm)	CO (ppm)
20	15	74.52	Actual value	276.01	31.97	25.39	16.17
			Predicted value	272.07	33.14	24.3	16.48
			Error (%)	1.44	-3.53	4.61	-1.86

for the diesel engine at 74.52% load and 15% EGR. The solution was chosen with a consensual value of 0.874, as shown in Figure 14. In addition, the highest value of BTE and the lowest value of BSFC, NO<sub>x</sub> emissions, and CO emissions combination were derived. The final predicted values of BTE, BSFC, NO<sub>x</sub> emissions, and CO emissions were 33.14%, 272.07g/(kWh), 24.3 ppm, and 16.48 ppm, respectively.

Based on response surface multi-objective optimization, it is concluded that diesel engines can be optimized to a considerable extent in terms of performance and emission characteristics when using an optimal biodiesel blending ratio of 20%. This optimization occurs especially at high engine loads and high EGR. The main reason for this is the desirable fuel properties of biodiesel, higher

oxygen content, and higher latent heat of vaporization contribute significantly to the optimal emission and combustion characteristics of the diesel engine (Ye et al., 2023).

### 5 Validation of optimization results

After the optimization results were obtained, the best solution obtained from the multi-objective optimization was returned to the simulation experiment for another validation to verify the correctness of the optimization results. Table 6 presents a comparison of the actual values corresponding to the optimal conditions of the engine biodiesel blending ratio, EGR, and

mixed load with the predicted values. The results show that the absolute errors in the predicted values of the model are consistent with an acceptable range. Thus, the developed model can accurately predict performance characteristics, and the absolute percentage error with the simulated values is less than 4%. However, in this paper, the percentage of absolute error is less than 5% for model predictions of NO<sub>x</sub> emission characteristics. This result may be due to the lack of experimental values and consensual values (Zuo et al., 2022). Finally, the validation results are in good agreement with the experimental data and can be used as a reference in the practical application of diesel engines.

## 6 Conclusion

In this paper, a response surface model was developed to study the effects of combustion and emission characteristics of diesel-biodiesel blends for diesel engines based on different engine blending ratios, loads, and EGR. The response surface model was developed with biodiesel blending ratio, load, and EGR as independent variables and BTE, BSFC, NO<sub>x</sub> emissions, and CO emissions as dependent variables. The maximum BTE, as well as the minimum BSFC, NO<sub>x</sub> emissions, and CO emissions, was obtained. The main findings are as follows:

- (1) The response models of EGR, biodiesel blending ratio, and load for BTE and BSFC show that load has the most significant effect on BTE and BSFC, and load has the greatest effect on diesel engine operation.
- (2) With increased EGR, the NO<sub>x</sub> emissions of diesel engines are significantly reduced, while NO<sub>x</sub> emissions increase with increases in the load and biodiesel blending ratio. It is possible that this is due to the recovery of heat energy by the EGR, which leads to a more complete combustion of the fuel, resulting in lower NO<sub>x</sub> emissions.
- (3) CO emissions decreased significantly with an increasing biodiesel blending ratio, which may be due to the increase of oxygen content, whereas the CO emissions increased with increasing load.
- (4) The best solution based on the response surface multi-objective optimization was selected as a consensual value of 0.874, using 20% biodiesel with 80% diesel as the fuel for the diesel engine at 74.52% load and 15% EGR. At this point, the BTE, BSFC, NO<sub>x</sub> emissions, and CO emissions were 33.14%, 272.07g/(kWh), 24.3 ppm, and 16.48 ppm, respectively.

This paper provides a better understanding of the relationship between EGR, biodiesel blending ratio, and load on the biodiesel

engine, and provides a reference for future research on the parameters of biodiesel engines and the development of EGR systems. In future work, more engine parameters and more efficient and refined optimization methods will be considered (Zhang et al., 2023b).

## Data availability statement

The original contributions presented in the study are included in the article/Supplementary Material; further inquiries can be directed to the corresponding author.

## Author contributions

JL: method, funding acquisition, conceptualization, and writing—review and editing; WZ: resources, project administration, method, software, data curation, writing—original draft, and writing—review and editing; JZ: data curation, and writing—review and editing; ZZ: software, formal analysis, investigation, and method; JH: investigation method, project administration, and formal analysis. All authors contributed to the article and approved the submitted version.

## Funding

The study was supported by the Ph.D. Programs Foundation of Guangxi University of Science and Technology (Grant No. 23Z04).

## Conflict of interest

The authors declare that the research was conducted in the absence of any commercial or financial relationships that could be construed as a potential conflict of interest.

## Publisher's note

All claims expressed in this article are solely those of the authors and do not necessarily represent those of their affiliated organizations, or those of the publisher, the editors, and the reviewers. Any product that may be evaluated in this article, or claim that may be made by its manufacturer, is not guaranteed or endorsed by the publisher.

## References

- Alaswad, A., Dassisti, M., Prescott, T., and Olabi, A. G. (2015). Technologies and developments of third generation biofuel production. *Renew. Sustain. Energy Rev.* 51, 1446–1460. doi:10.1016/j.rser.2015.07.058
- Cai, L., E, J. Q., Li, J., Ding, J., and Luo, B. (2023). A comprehensive review on combustion stabilization technologies of micro/meso-scale combustors for micro thermophotovoltaic systems: Thermal, emission, and energy conversion. *Fuel* 335, 126660. doi:10.1016/j.fuel.2022.126660
- Chen, Y. L., Chen, S. M., Tsai, J. M., Tsai, C. Y., Fang, H. H., Yang, I. C., et al. (2012). Optimization of suitable ethanol blend ratio for motorcycle engine using response surface method. *J. Environ. Sci. Health, Part A Toxic/Hazard. Subst. Environ. Eng.* 47 (1), 101–108. doi:10.1080/10934529.2012.629949
- Cui, S., Pang, S., Pang, D., Tian, F., and Yu, Y. (2022). The microstructure and pitting corrosion behavior of K-tig welded joints of the UNS S32101 duplex stainless steel. *MATERIALS* 16 (1), 250. doi:10.3390/ma16010250

- Cui, Y. F., Geng, Z. Q., Zhu, Q. X., and Han, Y. M. (2017). Review: Multi-objective optimization methods and application in energy saving. *Energy* 125, 681–704. doi:10.1016/j.energy.2017.02.174
- E, J., Pham, M., Zhao, D., Deng, Y. W., Le, D., Zuo, W., et al. (2017). Effect of different technologies on combustion and emissions of the diesel engine fueled with biodiesel: A review. *Renew. Sustain. Energy Rev.* 80, 620–647. doi:10.1016/j.rser.2017.05.250
- Elsayed, K., and Lacor, C. (2011). Modeling, analysis and optimization of aircyclones using artificial neural network, response surface methodology and CFD simulation approaches. *Powder Technol.* 212 (1), 115–133. doi:10.1016/j.powtec.2011.05.002
- Foley, A. M., Gallachoir, B. P. O., McKeogh, E. J., Milborrow, D., and Leahy, P. G. (2013). Addressing the technical and market challenges to high wind power integration in Ireland. *Renew. Sustain. Energy Rev.* 19, 692–703. doi:10.1016/j.rser.2012.11.039
- Guo, J. X., Zhuang, Y. B., Chen, L. M., Liu, J. H., Li, D. M., and Ye, N. H. (2012). Process optimization for microwave-assisted direct liquefaction of Sargassum polycystum C.Agarth using response surface methodology. *Bioresour. Technol.* 120, 19–25. doi:10.1016/j.biortech.2012.06.013
- Han, D., Deng, Y., Han, W., E, J. Q., Chen, L., Feng, C., et al. (2021). Effects analysis on hydrocarbon reduction efficiency of a beta zeolite catcher in gasoline engine during cold start. *Fuel* 306, 121614. doi:10.1016/j.fuel.2021.121614
- Hu, D., Wang, H., Wang, B., Shi, M., Duan, B., Wang, Y., et al. (2022a). Calibration of 0-D combustion model applied to dual-fuel engine. *Energy* 261, 125251. doi:10.1016/j.energy.2022.125251
- Hu, G. L., Zhou, F., Zhu, W. C., Yu, L. F., and Li, G. (2022b). Geometric optimization and performance analysis of radial MR valve using Taguchi orthogonal experiment method. *J. Mech. Sci. Technol.* 36 (9), 4593–4614. doi:10.1007/s12206-022-0822-2
- Hu, W., E, J. Q., Leng, E., Zhang, F., Chen, J., and Ma, Y. (2023). Investigation on harvesting characteristics of convective wind energy from vehicle driving on multi-lane highway. *Energy* 263, 126062. doi:10.1016/j.energy.2022.126062
- Jamaluddin, M. A., Ismail, K., Ishak, M. A. M., Ab Ghani, Z., Abdullah, M. F., Safian, M. T. U., et al. (2013). Microwave-assisted pyrolysis of palm kernel shell: Optimization using response surface methodology (RSM). *Renew. Energy* 55, 357–365. doi:10.1016/j.renene.2012.12.042
- Kashyap, D., Das, S., and Kalita, P. (2021). Exploring the efficiency and pollutant emission of a dual fuel CI engine using biodiesel and producer gas: An optimization approach using response surface methodology. *Sci. Total Environ.* 773, 145633. doi:10.1016/j.scitotenv.2021.145633
- Khare, A., Beckman, T., and Crouse, N. (2011). Cities addressing climate change: Introducing a tripartite model for sustainable partnership. *Sustain. Cities Soc.* 1 (4), 227–235. doi:10.1016/j.scs.2011.07.010
- Li, B., Wang, J., Zhang, H., Fan, L., Leng, X., Long, W., et al. (2023a). Multiple-objective optimization of Jet Controlled Compression Ignition (JCCI) mode with dual-direct injection in a high-speed light-duty engine. *Fuel* 333, 126327. doi:10.1016/j.fuel.2022.126327
- Li, Q., Hu, H., Ma, L. Y., Wang, Z. G., Arici, M., Li, D., et al. (2022). Evaluation of energy-saving retrofits for sunspace of rural residential buildings based on orthogonal experiment and entropy weight method. *Energy Sustain. Dev.* 70, 569–580. doi:10.1016/j.esd.2022.09.007
- Li, Y., Zhou, S., Liu, J., Tong, J., Dang, J., Yang, F., et al. (2023b). Multi-objective optimization of the Atkinson cycle gasoline engine using NSGA III coupled with support vector machine and back-propagation algorithm. *Energy* 262, 125262. doi:10.1016/j.energy.2022.125262
- Liu, Z., Luo, J., Pan, Y., Li, J., Li, L., Wei, X., et al. (2023). Multi-objective optimization of the performance and emission characteristics for a dual-fuel engine with hydrogen addition. *Fuel* 332, 126231. doi:10.1016/j.fuel.2022.126231
- Luo, J. B., Liu, Z. H., Wang, J., Xu, H. X., Tie, Y. H., Yang, D. Y., et al. (2022). Investigation of hydrogen addition on the combustion, performance, and emission characteristics of a heavy-duty engine fueled with diesel/natural gas. *Energy* 260, 125082. doi:10.1016/j.energy.2022.125082
- Martos, A., Pacheco-Torres, R., Ordonez, J., and Jadraque-Gago, E. (2016). Towards successful environmental performance of sustainable cities: Intervening sectors. A review. *Renew. Sustain. Energy Rev.* 57, 479–495. doi:10.1016/j.rser.2015.12.095
- Nuchitprasittichai, A., and Cremaschi, S. (2011). Optimization of CO2 capture process with aqueous amines using response surface methodology. *Comput. Chem. Eng.* 35 (8), 1521–1531. doi:10.1016/j.compchemeng.2011.03.016
- Ozgur, C. (2021). Optimization of biodiesel yield and diesel engine performance from waste cooking oil by response surface method (RSM). *Pet. Sci. Technol.* 39 (17–18), 1–21. doi:10.1080/10916466.2021.1954019
- Shahbaz, M., Yusup, S., Inayat, A., Patrick, D. O., and Pratama, A. (2016). Application of response surface methodology to investigate the effect of different variables on conversion of palm kernel shell in steam gasification using coal bottom ash. *Appl. Energy* 184, 1306–1315. doi:10.1016/j.apenergy.2016.05.045
- Shi, Z., Peng, Q., E, J. Q., Xie, B., Wei, J., Yin, R., et al. (2023). Mechanism, performance and modification methods for NH3-SCR catalysts: A review. *Fuel* 331, 125885. doi:10.1016/j.fuel.2022.125885
- Simssek, S., and Uslu, S. (2020). Investigation of the effects of biodiesel/2-ethylhexyl nitrate (EHN) fuel blends on diesel engine performance and emissions by response surface methodology (RSM). *Fuel* 275, 118005. doi:10.1016/j.fuel.2020.118005
- Singh, T. S., Rajak, U., Samuel, O. D., Chaurasiya, P. K., Natarajan, K., Verma, T. N., et al. (2021). Optimization of performance and emission parameters of direct injection diesel engine fuelled with microalgae Spirulina (L) - response surface methodology and full factorial method approach. *Fuel* 285, 119103. doi:10.1016/j.fuel.2020.119103
- Solmaz, H., Ardebili, S. M. S., Calam, A., Yilmaz, E., and Ipci, D. (2021). Prediction of performance and exhaust emissions of a CI engine fueled with multi-wall carbon nanotube doped biodiesel-diesel blends using response surface method. *Energy* 227, 120518. doi:10.1016/j.energy.2021.120518
- Sun, X., Kim, S., Yang, S. D., Kim, H. S., and Yoon, J. Y. (2017). Multi-objective optimization of a Stairmand cyclone separator using response surface methodology and computational fluid dynamics. *Powder Technol.* 320, 51–65. doi:10.1016/j.powtec.2017.06.065
- Tan, D. L., Meng, Y., Tian, J., Zhang, C., Zhang, Z., Yang, G., et al. (2023a). Utilization of renewable and sustainable diesel/methanol/n-butanol (DMB) blends for reducing the engine emissions in a diesel engine with different pre-injection strategies. *Energy* 269, 126785. doi:10.1016/j.energy.2023.126785
- Tan, D. L., Wu, Y., Lv, J. S., Li, J., Ou, X. Y., Meng, Y. J., et al. (2023b). Performance optimization of a diesel engine fueled with hydrogen/biodiesel with water addition based on the response surface methodology. *Energy* 263, 125869. doi:10.1016/j.energy.2022.125869
- Teng, T., and Qin, L. (2019). Analysis of regional environment and regional innovation strategy based on cybernetics. *Cogn. Syst. Res.* 57, 25–31. doi:10.1016/j.cogsys.2018.09.023
- Wang, C., Wang, C., Pan, H., and Yue, Y. (2022). Effect of structure parameters on low nitrogen performance of burner based on orthogonal experiment method. *Case Stud. Therm. Eng.* 39, 102404. doi:10.1016/j.csite.2022.102404
- Wang, Z. Q., and Li, L. J. (2022). Effect of pre-injection on combustion and emission characteristics of a diesel engine fueled with diesel/methanol/n-butanol blended fuel. *Processes* 10 (1), 60. doi:10.3390/pr10010060
- Ye, J. D., E, J. Q., and Peng, Q. (2023). Effects of porosity setting and multilayers of diesel particulate filter on the improvement of regeneration performance. *Energy* 263, 126063. doi:10.1016/j.energy.2022.126063
- Yilmaz, N., Atmanli, A., Hall, M. J., and Vigil, F. M. (2022). Determination of the optimum blend ratio of diesel, waste oil derived biodiesel and 1-pentanol using the response surface method. *Energies* 15 (14), 5144. doi:10.3390/en15145144
- Yu, H. L., Tarsitano, D., Hu, X. S., and Cheli, F. (2016). Real time energy management strategy for a fast charging electric urban bus powered by hybrid energy storage system. *Energy* 112, 322–331. doi:10.1016/j.energy.2016.06.084
- Yusup, S., Khan, Z., Ahmad, M. M., and Rashidi, N. A. (2014). Optimization of hydrogen production in *in-situ* catalytic adsorption (ICA) steam gasification based on Response Surface Methodology. *Biomass Bioenergy* 60, 98–107. doi:10.1016/j.biombioe.2013.11.007
- Zhang, B., Li, X. W., Zuo, Q. S., Yin, Z. B., Zhang, J. P., Chen, W., et al. (2022a). Effects analysis on hydrocarbon light-off performance of a catalytic gasoline particulate filter during cold start. *Environ. Sci. Pollut. Res.* 29 (51), 76890–76906. doi:10.1007/s11356-022-20519-0
- Zhang, B., Li, X. W., Wan, Q., Liu, B., Jia, G. H., and Yin, Z. B. (2023a). Hydrocarbon emission control of an adsorptive catalytic gasoline particulate filter during cold-start period of the gasoline engine. *Energy* 262, 125445. doi:10.1016/j.energy.2022.125445
- Zhang, Y. H., Zhong, Y. H., Wang, J., Tan, D. L., Zhang, Z. Q., and Yang, D. Y. (2021a). Effects of different biodiesel-diesel blend fuel on combustion and emission characteristics of a diesel engine. *Processes* 9 (11), 1984. doi:10.3390/pr9111984
- Zhang, Z. Q., Dong, R., Lan, G., Yuan, T., and Tan, D. L. (2023b). Diesel particulate filter regeneration mechanism of modern automobile engines and methods of reducing PM emissions: A review. *Environ. Sci. Pollut. Res.* 30 (14), 39338–39376. doi:10.1007/s11356-023-25579-4
- Zhang, Z. Q., Dong, R., Tan, D. L., Duan, L., Jiang, F., Yao, X. X., et al. (2023c). Effect of structural parameters on diesel particulate filter trapping performance of heavy-duty diesel engines based on grey correlation analysis. *Energy* 271, 127025. doi:10.1016/j.energy.2023.127025
- Zhang, Z. Q., Li, J. T., Tian, J., Dong, R., Zou, Z., Gao, S., et al. (2022b). Performance, combustion and emission characteristics investigations on a diesel engine fueled with diesel/ethanol/n-butanol blends. *Energy* 249, 123733. doi:10.1016/j.energy.2022.123733
- Zhang, Z. Q., Lv, J. S., Li, W. Q., Long, J. M., Wang, S., Tan, D. L., et al. (2022c). Performance and emission evaluation of a marine diesel engine fueled with natural gas ignited by biodiesel-diesel blended fuel. *Energy* 256, 124662. doi:10.1016/j.energy.2022.124662

- Zhang, Z. Q., Lv, J. S., Xie, G. L., Wang, S., Ye, Y. S., Huang, G. H., et al. (2022d). Effect of assisted hydrogen on combustion and emission characteristics of a diesel engine fueled with biodiesel. *Energy* 254, 124269. doi:10.1016/j.energy.2022.124269
- Zhang, Z. Q., Tian, J., Xie, G. L., Li, J. T., Xu, W. B., Jiang, F., et al. (2022e). Investigation on the combustion and -emission characteristics of diesel engine fueled with diesel/methanol/n-butanol blends. *Fuel* 314, 123088. doi:10.1016/j.fuel.2021.123088
- Zhang, Z. Q., Ye, J. D., Tan, D. L., Feng, Z. Q., Luo, J. B., Tan, Y., et al. (2021b). The effects of Fe<sub>2</sub>O<sub>3</sub> based DOC and SCR catalyst on the combustion and emission characteristics of a diesel engine fueled with biodiesel. *Fuel* 290, 120039. doi:10.1016/j.fuel.2020.120039
- Zhao, X. H., E, J. Q., Liao, G. L., Zhang, F., Chen, J. W., and Deng, Y. W. (2021). Numerical simulation study on soot continuous regeneration combustion model of diesel particulate filter under exhaust gas heavy load. *Fuel* 290, 119795. doi:10.1016/j.fuel.2020.119795
- Zhao, X. H., Jiang, J., Zuo, H. Y., and Jia, G. H. (2023). Soot combustion characteristics of oxygen concentration and regeneration temperature effect on continuous pulsation regeneration in diesel particulate filter for heavy-duty truck. *Energy* 264, 126265. doi:10.1016/j.energy.2022.126265
- Zhao, X. H., Zuo, H. Y., and Jia, G. H. (2022). Effect analysis on pressure sensitivity performance of diesel particulate filter for heavy-duty truck diesel engine by the nonlinear soot regeneration combustion pressure model. *Energy* 257, 124766. doi:10.1016/j.energy.2022.124766
- Zuo, H. Y., Zhu, Y., Wu, S., Abubakar, S., and Li, Y. (2022). Effect of a crossed-semicircular-plate on thermal performance of micro-combustor fueled by premixed hydrogen-air mixture. *Int. J. Hydrogen Energy* 47 (39), 17442–17453. doi:10.1016/j.ijhydene.2022.03.212